ETH
Eidgenössische Technische Hochschule Zürich
Swiss Federal Institute of Technology Zurich

Seminar for Applied Mathematics SAM

A fully-coupled subwavelength resonance approach to modelling the passive cochlea

H. Ammari and B. Davies

Research Report No. 2019-09

January 2019
Latest revision: March 2019

Seminar für Angewandte Mathematik
Eidgenössische Technische Hochschule
CH-8092 Zürich
Switzerland

A fully-coupled subwavelength resonance approach to modelling the passive cochlea

Habib Ammari* Bryn Davies*

Abstract

The aim of this paper is to understand the behaviour of a large number of coupled subwavelength resonators. We use layer potential techniques in combination with numerical computations to study the acoustic pressure field due to scattering by a graded array of subwavelength resonators. Our set-up is designed to model the structure of cochlear hair cells on the surface of the basilar membrane. We compute the resonant modes of the system and explore the model's ability to decompose incoming signals. Significantly, we are able to offer a mathematical explanation for the cochlea's so-called "travelling wave" behaviour and tonotopic frequency map.

Mathematics subject classification: 35R30, 35C20
Keywords: subwavelength resonance, cochlear mechanics, coupled resonators, hybridisation, passive cochlea, signal processing

1 Introduction

The development of the understanding of the cochlea has largely been a dichotomy between two classes of models [11]. The first, proposed by Hermann von Helmholtz in the 1850s, are based on resonators tuned to different audible frequencies being distributed along the length of the cochlea [25]. Later, Georg von Békésy demonstrated that when the cochlea is stimulated a wave travels from the base to the apex along the basilar membrane [24]. This discovery won him a Nobel Prize in 1961 and lead to the creation of models based on each receptor cell being excited in sequence as the signal travels through the cochlea.

More recent developments have put Helmholtz' resonance model back in the spotlight by identifying bundles of cells known as inner hair cells as candidate resonant elements. These cells are 20-70µm tall and are distributed along the basilar membrane increasing in size from base to apex [15, 22]. It is now known that the displacement of a hair cell bundle leads to a change in the distribution

*Department of Mathematics, ETH Zürich, Rämistrasse 101, CH-8092 Zürich, Switzerland (habib.ammari@sam.math.ethz.ch, bryn.davies@sam.math.ethz.ch).

of electrical charge in the cell membrane [17], offering a mechanism for the production of a signal in the auditory nerve.

It is also known that the cochlea is an active organ and emits sounds (known as otoacoustic emissions) as part of its response to a signal [13, 18, 19]. We shall only consider a passive system of resonators here, but will present a model that can be readily modified to include active elements in future work.

In this paper, we apply boundary integral techniques to understand the complex interactions between the hair cell bundles [5, 10]. A human cochlea has around 3500 inner hair cells and is approximately 30mm long [20]. Compare this to the wavelength of audible sound (a few centimetres to several metres) and it is clear that complex interactions will occur between the resonant elements, the mathematical complexity of which has been the main barrier to developing Helmholtz' resonance models.

In order to study the coupling interactions between hair cell bundles we will model the acoustic pressure on the surface of the basilar membrane. We will thus consider the problem of acoustic wave scattering by compressible elements in two-dimensional space. In [12, Chap. 8] Bell presents a thorough discussion of the evidence supporting modelling (living) hair cells as compressible elements that have material parameters closer to that of air than water. In particular, the high Poisson ratio of hair cells is cited as compelling evidence against the assumption that hair cells are incompressible [1, §3.2.2]. The assumption that there is a high contrast between both the material parameters of the cell bundles and the cochlear fluid is central to our analysis. Similar techniques have previously been applied to other high-contrast materials that exhibit subwavelength resonance, the classical example being the Minnaert resonance of air bubbles in water [3, 5]. This analysis (in Sections 2.2 & 2.3) relies on the use of layer potential techniques [4, 7, 9].

It is found that a graded array of hybridised resonators has a set of resonant frequencies that becomes increasingly dense (within a finite range) as the number of resonators is increased. We study the eigenmodes and present a scheme (in Section 2.4) for how the model processes incoming signals, filtering them into the system's resonant frequencies. Finally, in Sections 2.5 & 2.6 we present the significant observations that our (resonance) model predicts the existence of a travelling wave in the pressure field and a basis for the tonotopic map. This acoustic pressure wave is complementary to the wave seen in the motion of the basilar membrane by Békésy and has been observed experimentally [21]. It is important to note that these observations are based solely on modelling the acoustic pressure on the surface of the basilar membrane, the motion of the membrane itself is not considered in this work.

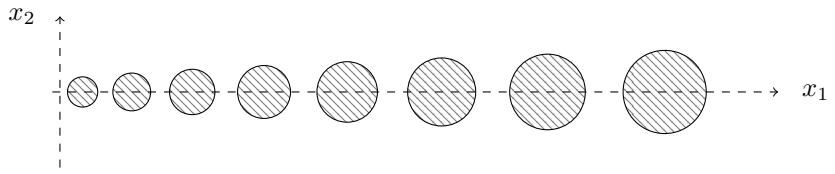

Figure 1: An array of eight (circular) subdomains $D = D_1 \cup \cdots \cup D_8$ graded in size and arranged linearly along $x_2 = 0$.

2 Response of the coupled resonators

2.1 Preliminaries

We consider a domain D in $\mathbb{R}^2$ which is the disjoint union of $N \in \mathbb{N}$ bounded and simply connected subdomains $\{D_1, \ldots, D_N\}$ such that, for each $n = 1, \ldots, N$, there is $0 < s < 1$ so that $\partial D_n \in C^{1,s}$ (that is, each ∂D_n is locally the graph of a differentiable function whose derivatives are Hölder continuous with exponent s). These disjoint subdomains represent the N hair cell bundles. We will consider the bundles arranged in a straight line since the curvature of the cochlea does not contribute to its mechanical behaviour [15]. Figure 1 shows an example of such an arrangement (in the special case of circular subdomains, which we will consider from Section 2.3 onwards).

We denote by ρ_b and κ_b the density and bulk modulus of the interior of the cell bundles, respectively, and denote by ρ and κ the corresponding parameters for the auditory fluid (which we assume occupies $\mathbb{R}^2 \setminus \overline{D}$).

We consider an incident acoustic pressure wave $p^{in}(x,t)$ (where $x = (x_1, x_2) \in \mathbb{R}^2$ and $t \in \mathbb{R}$) that is scattered by D. This problem is given by

$$\begin{cases} \left(\nabla \cdot \frac{1}{\rho}\nabla - \frac{1}{\kappa}\frac{\partial^2}{\partial t^2}\right) p = 0, & \text{for } (x,t) \in \mathbb{R}^2 \setminus \overline{D} \times \mathbb{R}, \\ \left(\nabla \cdot \frac{1}{\rho_b}\nabla - \frac{1}{\kappa_b}\frac{\partial^2}{\partial t^2}\right) p = 0, & \text{for } (x,t) \in D \times \mathbb{R}, \\ p_+ - p_- = 0, & \text{for } (x,t) \in \partial D \times \mathbb{R}, \\ \frac{1}{\rho}\frac{\partial p}{\partial \nu_x}\big|_+ - \frac{1}{\rho_b}\frac{\partial p}{\partial \nu_x}\big|_- = 0, & \text{for } (x,t) \in \partial D \times \mathbb{R}, \\ p^s := p - p^{in} = 0, & \text{for } x \in \mathbb{R}^2, t \ll 0, \end{cases} \tag{1}$$

where $\frac{\partial}{\partial \nu_x}$ denotes the outward normal derivative in x and the subscripts + and - are used to denote evaluation from outside and inside ∂D respectively.

We then introduce the auxiliary parameters

$$v = \sqrt{\frac{\kappa}{\rho}}, \quad v_b = \sqrt{\frac{\kappa_b}{\rho_b}}, \quad k = \frac{\omega}{v}, \quad k_b = \frac{\omega}{v_b},$$

which are the wave speeds and wavenumbers in $\mathbb{R}^2 \setminus \overline{D}$ and in D respectively. We also introduce the two dimensionless contrast parameters

$$\delta = \frac{\rho_b}{\rho}, \quad \tau = \frac{k_b}{k} = \frac{v_b}{v} = \sqrt{\frac{\rho\kappa_b}{\rho_b\kappa}}. \tag{2}$$

By rescaling the dimensions of the physical problem we can assume that

$$v = O(1), \quad v_b = O(1), \quad \tau = O(1). \tag{3}$$

We also assume that the rescaled dimensions are such that the subdomains $\{D_1, \ldots, D_N\}$ have widths that are $O(1)$. On the other hand, we assume that there is a large contrast between both the bulk moduli and the density, so that

$$\delta \ll 1. \tag{4}$$

Such an assumption is explored at length in [12], relying on experimental determinations of the Poisson ratio of hair cells.

We transform problem (1) into the complex frequency domain by making the transformation $u(x,\omega) := \int_{-\infty}^{\infty} p(x,t)e^{i\omega t}\,dt$, $\omega \in \mathbb{C}$ to reach

$$\begin{cases} \left(\Delta + k^2\right) u(x,\omega) = 0, & \text{in } \mathbb{R}^2 \setminus \overline{D}, \\ \left(\Delta + k_b^2\right) u(x,\omega) = 0, & \text{in } D, \\ u_+ - u_- = 0, & \text{on } \partial D, \\ \delta \frac{\partial u}{\partial \nu}\big|_+ - \frac{\partial u}{\partial \nu}\big|_- = 0, & \text{on } \partial D, \\ u^s := u - u^{in} \text{ satisfies the SRC}, & \text{as } |x| \to \infty. \end{cases} \tag{5}$$

'SRC' is used to denote the Sommerfeld radiation condition

$$\lim_{|x|\to\infty} |x|^{1/2} \left(\frac{\partial}{\partial |x|} - ik \right) u(x,\omega) = 0. \tag{6}$$

The SRC is the condition required to ensure that we select the solution that is outgoing (rather than incoming from infinity) and gives the well-posedness of problem (5).

We wish to use layer potential representations for the solutions to the scattering problem (5).

Definition 2.1. *We define the Helmholtz single layer potential associated with the domain D and wavenumber k as*

$$\mathcal{S}_D^k[\varphi](x) := \int_{\partial D} \Gamma^k(x-y)\varphi(y)\,d\sigma(y), \quad x \in \partial D, \varphi \in L^2(\partial D), \tag{7}$$

where Γ^k is the outgoing (i.e. satisfying the SRC) fundamental solution to the Helmholtz operator $\Delta + k^2$ in $\mathbb{R}^2$. We similarly define the Neumann-Poincaré operator associated with D and k as

$$\mathcal{K}_D^{k,*}[\varphi](x) = \int_{\partial D} \frac{\partial \Gamma^k(x-y)}{\partial \nu_x} \varphi(y)\,d\sigma(y), \quad x \in \partial D, \varphi \in L^2(\partial D). \tag{8}$$

We can then represent the solution to (5) as

$$u = \begin{cases} u^{in}(x) + \mathcal{S}_D^k[\psi](x), & x \in \mathbb{R}^2 \setminus \overline{D}, \\ \mathcal{S}_D^{k_b}[\phi](x), & x \in D, \end{cases} \tag{9}$$

for some surface potentials $(\phi, \psi) \in L^2(\partial D) \times L^2(\partial D)$.

We define the space $H^1(\partial D) := \{u \in L^2(\partial D) : \nabla u \in L^2(\partial D)\}$ in the usual way and use Id to denote the identity on $L^2(\partial D)$. Then, using the representation (9), problem (5) is equivalent [7, 9] to finding $(\phi, \psi) \in L^2(\partial D) \times L^2(\partial D)$ such that

$$\mathcal{A}(\omega, \delta) \begin{pmatrix} \phi \\ \psi \end{pmatrix} = \begin{pmatrix} u^{in} \\ \delta \frac{\partial u^{in}}{\partial \nu_x} \end{pmatrix}, \tag{10}$$

where

$$\mathcal{A}(\omega, \delta) := \begin{bmatrix} \mathcal{S}_D^{k_b} & -\mathcal{S}_D^{k} \\ -\frac{1}{2}Id + \mathcal{K}_D^{k_b,*} & -\delta(\frac{1}{2}Id + \mathcal{K}_D^{k,*}) \end{bmatrix}. \tag{11}$$

We now recall from *e.g.* [3, 4] the main result that will allow us to understand the leading order behaviour of $\mathcal{A}$ in (10).

Lemma 2.2. *In the space* $\mathcal{L}(L^2(\partial D) \times L^2(\partial D), H^1(\partial D) \times L^2(\partial D))$ *we have*

$$\mathcal{A}(\omega, \delta) = \mathcal{A}_0 + \omega^2 \ln \omega \mathcal{A}_{1,1,0} + \omega^2 \mathcal{A}_{1,2,0} + \delta \mathcal{A}_{0,1} + O(\delta \omega^2 \ln \omega) + O(\omega^4 \ln \omega),$$

where

$$\mathcal{A}_0 := \begin{bmatrix} \hat{\mathcal{S}}_D^{k_b} & -\hat{\mathcal{S}}_D^{k} \\ -\frac{1}{2}Id + \mathcal{K}_D^{*} & 0 \end{bmatrix}, \mathcal{A}_{1,1,0} := \begin{bmatrix} v_b^{-2}\mathcal{S}_{D,1}^{(1)} & -v^{-2}\mathcal{S}_{D,1}^{(1)} \\ v_b^{-2}\mathcal{K}_{D,1}^{(1)} & 0 \end{bmatrix},$$

$$\mathcal{A}_{1,2,0} := \begin{bmatrix} v_b^{-2}(-\ln v_b \mathcal{S}_{D,1}^{(1)} + \mathcal{S}_{D,1}^{(2)}) & -v^{-2}(-\ln v \mathcal{S}_{D,1}^{(1)} + \mathcal{S}_{D,1}^{(2)}) \\ v_b^{-2}(-\ln v_b \mathcal{K}_{D,1}^{(1)} + \mathcal{K}_{D,1}^{(2)}) & 0 \end{bmatrix},$$

and

$$\mathcal{A}_{0,1} := \begin{bmatrix} 0 & 0 \\ 0 & -(\frac{1}{2}Id + \mathcal{K}_D^{*}) \end{bmatrix}.$$

The above operators are defined as

$$\mathcal{S}_D[\phi](x) := \frac{1}{2\pi} \int_{\partial D} \ln|x-y| \phi(y)\, d\sigma(y),$$

$$\hat{\mathcal{S}}_D^{k}[\phi](x) := \mathcal{S}_D[\phi](x) + \eta_k \int_{\partial D} \phi\, d\sigma, \quad \eta_k := \frac{1}{2\pi}(\ln k + \gamma - \ln 2) - \frac{i}{4},$$

$$\mathcal{S}_{D,1}^{(1)}[\phi](x) := \int_{\partial D} b_1 |x-y|^2 \phi(y)\, d\sigma(y),$$

$$\mathcal{S}_{D,1}^{(2)}[\phi](x) := \int_{\partial D} b_1 |x-y|^2 \ln|x-y| \phi(y) + c_1 |x-y|^2 \phi(y)\, d\sigma(y),$$

$$\mathcal{K}_{D,1}^{(1)}[\phi](x) := \int_{\partial D} b_1 \frac{\partial |x-y|^2}{\partial \nu(x)} \phi(y)\, d\sigma(y),$$

$$\mathcal{K}_{D,1}^{(2)}[\phi](x) := \int_{\partial D} b_1 \frac{\partial |x-y|^2 \ln|x-y|}{\partial \nu(x)} \phi(y) + c_1 \frac{\partial |x-y|^2}{\partial \nu(x)} \phi(y)\, d\sigma(y),$$

where $b_1 := -\frac{1}{8\pi}$, $c_1 := -\frac{1}{8\pi}(\gamma - \ln 2 - 1 - \frac{i\pi}{2})$ *and* $\gamma = 0.5772\ldots$ *is the Euler constant.*

The operator $\mathcal{S}_D$ is the Laplace single layer potential associated with D. Since we are working in two dimensions this is not generally invertible however the following two lemmas help us understand the extent of its degeneracy.

Lemma 2.3. *If for some $\phi \in L^2(\partial D)$ with $\int_{\partial D} \phi = 0$ it holds that $\mathcal{S}_D[\phi](x) = 0$ for all $x \in \partial D$, then $\phi = 0$ on ∂D.*

Proof. The arguments given in [8, Lemma 2.25] can be easily generalised to the case where D is the disjoint union of a finite number of bounded Lipschitz domains in $\mathbb{R}^2$. □

Proposition 2.4. *Independent of the number $N \in \mathbb{N}$ of connected components making up D, we have that*

$$\dim \ker \mathcal{S}_D \leq 1.$$

Proof. Let $\psi \in \ker \mathcal{S}_D$. Then by Lemma 2.3 if $\int_{\partial D} \psi = 0$ then $\psi = 0$. Suppose that $\int_{\partial D} \psi \neq 0$ then take $\tilde{\psi} \in \ker \mathcal{S}_D$ with $\int_{\partial D} \tilde{\psi} \neq 0$ and then consider the function

$$f = \frac{\psi}{\int_{\partial D} \psi} - \frac{\tilde{\psi}}{\int_{\partial D} \tilde{\psi}}.$$

Then f satisfies $\mathcal{S}_D[f] = 0$ and $\int_{\partial D} f = 0$ so by Lemma 2.3 we have that $f = 0$. Therefore $\psi = (\int_{\partial D} \psi / \int_{\partial D} \tilde{\psi})\tilde{\psi}$. □

There are two cases to consider, in light of Proposition 2.4:

- Case I: $\dim \ker \mathcal{S}_D = 1$,
- Case II: $\dim \ker \mathcal{S}_D = 0$.

By the Fredholm Alternative Theorem, an equivalent formulation is

- Case I: $\mathcal{S}_D$ is not invertible,
- Case II: $\mathcal{S}_D$ is invertible.

as an operator in $\mathcal{L}(L^2(\partial D), H^1(\partial D))$. We are now in a position to prove an important property of the operator $\hat{\mathcal{S}}_D^k$ that was defined in Lemma 2.2 and is the leading order approximation to $\mathcal{S}_D^k$.

Lemma 2.5. *For any fixed $k \in \mathbb{C}\backslash\{0\}$, $\hat{\mathcal{S}}_D^k$ is invertible in $\mathcal{L}(L^2(\partial D), H^1(\partial D))$.*

Proof. Since $\hat{\mathcal{S}}_D^k$ is Fredholm with index 0 we need only to show that it is injective. To this end, assume that $y \in L^2(\partial D)$ is such that

$$\hat{\mathcal{S}}_D^k[y] = \mathcal{S}_D[y] + \eta_k \int_{\partial D} y = 0. \tag{12}$$

Case I: Let ψ_0 be the unique element of $\ker \mathcal{S}_D$ with $\int_{\partial D} \psi_0 = 1$ (which exists as a result of Lemma 2.3). We then find that $\mathcal{S}_D[y] \perp \psi_0$ in $L^2(\partial D)$ and hence (12) becomes

$$\eta_k \left(\int_{\partial D} y \right) \left(\int_{\partial D} \psi_0 \right) = 0.$$

Thus $\int_{\partial D} y = 0$. It follows from (12) that $\mathcal{S}_D[y] = 0$ and further by Lemma 2.3 we have that $y = 0$.
Case II: Define $\psi_0 = \mathcal{S}_D^{-1}(1)$ then (12) gives us that

$$\mathcal{S}_D[y] = -\eta_k \int_{\partial D} y,$$

is constant so, since $\mathcal{S}_D$ is injective, we find that $y = c\psi_0$ for some c. Substituting back into (12) gives

$$c + \eta_k c \int_{\partial D} \psi_0 = 0.$$

Everything here is real with the one exception of η_k (which has nonzero imaginary part) so we must have that $c = 0$. □

2.2 Resonant modes

Definition 2.6. *For a fixed δ we define a resonant frequency to be $\omega \in \mathbb{C}$ with positive real part and negative imaginary part such that there exists a nontrivial solution to*

$$\mathcal{A}(\omega, \delta) \begin{pmatrix} \phi \\ \psi \end{pmatrix} = \begin{pmatrix} 0 \\ 0 \end{pmatrix}, \tag{13}$$

where $\mathcal{A}(\omega, \delta)$ is defined in (11). For each resonant frequency ω we define the corresponding eigenmode (or resonant mode or normal mode) as

$$u = \begin{cases} \mathcal{S}_D^k[\psi](x), & x \in \mathbb{R}^2 \backslash D, \\ \mathcal{S}_D^{k_b}[\phi](x), & x \in D. \end{cases} \tag{14}$$

Remark 2.7. *The reason for the choices of sign in Definition 2.6 is to give a physical meaning to a complex resonant frequency. The real part represents the frequency of oscillation and the imaginary part describes the rate of attenuation (hence it should be negative, to give a solution that decays over time).*

Remark 2.8. *We will see from Figure 4 that Definition 2.6 is equivalent to the notion that resonant frequencies are those at which the system will oscillate at much greater amplitude than is generally the case.*

We wish to now compute the resonant frequencies and associated eigenmodes for our system. Manipulating the first entry of (13) we find that

$$\hat{\mathcal{S}}_D^{k_b}[\phi] - \hat{\mathcal{S}}_D^k[\psi] = \hat{\mathcal{S}}_D^k[\phi - \psi] + \frac{1}{2\pi} \ln \frac{v}{v_b} \int_{\partial D} \phi,$$

hence

$$\psi = \phi + \frac{1}{2\pi} \ln \frac{v}{v_b} \left(\int_{\partial D} \phi \right) (\hat{\mathcal{S}}_D^k)^{-1}[\chi_{\partial D}] + O(\omega^2), \tag{15}$$

since an application of $(\hat{\mathcal{S}}_D^k)^{-1}$ rescales like $O(1/\ln \omega)$. Here, $\chi_{\partial D}$ is used to denote the characteristic function of ∂D.

To deal with the second component of (13) we first prove some technical lemmas.

Lemma 2.9. *For any $\phi \in L^2(\partial D)$ and $j = 1, \ldots, N$, we have that*
(i) $\int_{\partial D_j} (\frac{1}{2} I - \mathcal{K}_D^*)[\phi] = 0$,
(ii) $\int_{\partial D_j} (\frac{1}{2} I + \mathcal{K}_D^*)[\phi] = \int_{\partial D_j} \phi$.

Proof. (i) follows from the jump relations for single layer potentials and the fact $\mathcal{S}_D[\phi]$ is harmonic in D [8, 9]. Then (ii) is immediate. □

Lemma 2.10. *For any $\phi \in L^2(\partial D)$ and $j = 1, \ldots, N$, we have that*
(i) $\int_{\partial D_j} \mathcal{K}_{D,1}^{(1)}[\phi] = 4b_1 |D_j| \int_{\partial D} \phi$,
(ii) $\int_{\partial D_j} \mathcal{K}_{D,1}^{(2)}[\phi] = -\int_{D_j} \mathcal{S}_D[\phi] + (4b_1 + 4c_1)|D_j| \int_{\partial D} \phi$,
where $|D_i|$ is the area of D_i.

Proof. (i) follows from the divergence theorem

$$\begin{aligned}\int_{\partial D_j} \mathcal{K}_{D,1}^{(1)}[\phi](x)\, d\sigma(x) &= b_1 \int_{D_j} \int_{\partial D} \Delta_x |x-y|^2 \phi(y)\, d\sigma(y)\, dx \\ &= 4b_1 |D_j| \int_{\partial D} \phi(y)\, d\sigma(y).\end{aligned}$$

Similarly for (ii) we can show that

$$\begin{aligned}\int_{\partial D_j} K_{D,1}^{(2)}[\phi](x)\, d\sigma(x) &= \int_{D_j} \int_{\partial D} \Delta_x [|x-y|^2 (b_1 \ln|x-y| + c_1)] \phi(y)\, d\sigma(y)\, dx \\ &= -\int_{D_j} \mathcal{S}_D[\phi](x)\, dx + (4b_1 + 4c_1)|D_j| \int_{\partial D} \phi(y)\, d\sigma(y),\end{aligned}$$

making use of the fact that $b_1 = -1/8\pi$. □

Turning now to the second component of (13) we see that

$$\begin{aligned}\left(-\frac{1}{2} Id + \mathcal{K}_D^* + v_b^{-2} \mathcal{K}_{D,1}^{(1)} \omega^2 \ln\omega + v_b^{-2} (-\ln v_b \mathcal{K}_{D,1}^{(1)} + \mathcal{S}_{D,1}^{(2)}) \omega^2 \right)[\phi] \\ -\delta (\frac{1}{2} Id + \mathcal{K}_D^*)[\psi] = O(\delta \omega^2 \ln\omega) + O(\omega^4 \ln\omega).\end{aligned}$$

We substitute expression (15) for ψ to see that ϕ satisfies the equation

$$\begin{aligned}\left(-\frac{1}{2} Id + \mathcal{K}_D^* \right)[\phi] + \left(v_b^{-2} \mathcal{K}_{D,1}^{(1)} \omega^2 \ln\omega + v_b^{-2} (-\ln v_b \mathcal{K}_{D,1}^{(1)} + \mathcal{K}_{D,1}^{(2)}) \omega^2 \right)[\phi] \\ -\delta (\frac{1}{2} Id + \mathcal{K}_D^*)[\phi] - \frac{1}{2\pi} \delta \ln \frac{v}{v_b} \left(\int_{\partial D} \phi \right) \left(\frac{1}{2} Id + \mathcal{K}_D^* \right) \left[(\hat{\mathcal{S}}_D^k)^{-1} [\chi_{\partial D}] \right] \\ = O(\delta \omega^2 \ln\omega) + O(\omega^4 \ln\omega).\end{aligned} \tag{16}$$

At leading order (16) is just $(-\frac{1}{2} Id + \mathcal{K}_D^*)[\phi] = 0$ so it would be useful to understand this kernel, which we achieve with the following two lemmas.

Lemma 2.11. *If $\phi \in L^2(\partial D)$ is such that $\phi \in \ker(-\frac{1}{2}Id + \mathcal{K}_D^*)$ then there exist constants b_j such that $\mathcal{S}_D[\phi] = \sum_{j=1}^N b_j \mathcal{X}_{\partial D_j}$.*

Proof. Let $u := \mathcal{S}_D[\phi]$. Then $\Delta u = 0$ in D and $\frac{\partial u}{\partial \nu}\big|_- = (-\frac{1}{2}Id + \mathcal{K}_D^*)[\phi] = 0$ on ∂D (known as a "jump condition") [7, 9] so u satisfies a homogeneous interior Neumann problem on each of the N connected components $D_1, \ldots, D_N$ of D. It is known that such problems are uniquely solvable up to the addition of a constant. □

Lemma 2.12. *Fix some $k_0 \in \mathbb{C} \setminus \{0\}$. The set of vectors $\{\psi_1, \ldots, \psi_N\}$ defined as*

$$\psi_i := \left(\hat{\mathcal{S}}_D^{k_0}\right)^{-1} [\mathcal{X}_{\partial D_i}], \tag{17}$$

forms a basis for the space $\ker(-\frac{1}{2}Id + \mathcal{K}_D^*)$.

Proof. The linear independence of $\{\psi_1, \ldots, \psi_N\}$ follows from the linearity and injectivity of $\hat{\mathcal{S}}_D^{k_0}$, plus the independence of $\{\mathcal{X}_{\partial D_1}, \ldots, \mathcal{X}_{\partial D_N}\}$.

For $\phi \in L^2(\partial D)$ the difference between $\hat{\mathcal{S}}_D^{k_0}[\phi](x)$ and $\mathcal{S}_D[\phi](x)$ is a constant (in x) so they will have the same derivatives. In particular, they are both harmonic and satisfy the same jump conditions across ∂D. Therefore, using arguments as in Lemma 2.11, we see that if $\phi \in \ker(-\frac{1}{2}Id + \mathcal{K}_D^*)$ then $\hat{\mathcal{S}}_D^{k_0}[\phi] \in \operatorname{span}\{\mathcal{X}_{\partial D_1}, \ldots, \mathcal{X}_{\partial D_N}\}$. Thus $\phi \in \operatorname{span}\{\psi_1, \ldots, \psi_N\}$. □

From Lemma 2.12 we know that $\ker(-\frac{1}{2}Id + \mathcal{K}_D^*)$ has dimension equal to the number of connected components of D (a wider discussion can be found in *e.g.* [2]). Thus we can take a basis

$$\{\phi_1, \ldots, \phi_N\},$$

of the null space $\ker(-\frac{1}{2}Id + \mathcal{K}_D^*)$. Then, in light of the fact that at leading order (16) is just $(-\frac{1}{2}Id + \mathcal{K}_D^*)[\phi] = 0$, it is natural to seek a solution of the form

$$\phi = \sum_{j=1}^N a_j \phi_j + O(\omega^2 \ln \omega + \delta), \tag{18}$$

for some non-trivial constants a_j with $\sum_j |a_j| = O(1)$. The solutions (ϕ, ψ) to (13) are determined only up to multiplication by a constant (and hence so are $a_1, \ldots, a_N$). We fix the scaling to be such that the eigenmodes are normalised in the $L^2(D)$-norm

$$\|u\|^2_{L^2(D)} = \int_D |\mathcal{S}_D^{k_b}[\phi]|^2 = 1. \tag{19}$$

We now integrate (16) over each $\partial D_i, i = 1 \ldots N$ and use the results of Lemmas 2.9 and 2.10 to find that, up to an error of $O(\delta\omega^2 \ln \omega) + O(\omega^4 \ln \omega)$,

$$B_\delta^{(i)}(\omega)[\phi] := \left(\int_{\partial D}\phi\right)\left(\omega^2\ln\omega + \left(\left(1+\frac{c_1}{b_1}-\ln v_b\right) - \frac{\mathcal{S}_D[\phi]|_{\partial D_i}}{4b_1(\int_{\partial D}\phi)}\right)\omega^2\right) - \frac{v_b^2}{4b_1|D_i|}\left[\int_{\partial D_i}\phi + \frac{\ln(v/v_b)}{2\pi}\left(\int_{\partial D}\phi\right)\int_{\partial D_i}(\hat{\mathcal{S}}_D^k)^{-1}[\chi_{\partial D}]\right]\delta = 0. \tag{20}$$

When we substitute the expression (18) for ϕ in (20) we find the system of equations, up to an error of order $O(\delta\omega^2\ln\omega)+O(\omega^4\ln\omega)$,

$$\begin{pmatrix} B_\delta^{(1)}(\omega)[\phi_1] & B_\delta^{(1)}(\omega)[\phi_2] & \dots & B_\delta^{(1)}(\omega)[\phi_N] \\ \vdots & \vdots & \ddots & \vdots \\ B_\delta^{(N)}(\omega)[\phi_1] & B_\delta^{(N)}(\omega)[\phi_2] & \dots & B_\delta^{(N)}(\omega)[\phi_N] \end{pmatrix}\begin{pmatrix} a_1 \\ \vdots \\ a_N \end{pmatrix} = 0. \tag{21}$$

Remark 2.13. *Thanks to the linearity of the operators $B_\delta^{(i)}$, the solutions $\omega(\delta)$ to* (21) *(as well as the associated eigenmodes) are independent of the choice of basis $\{\phi_1,\dots,\phi_N\}$.*

Remark 2.14. *One can think of the step where we integrated* (16) *over each ∂D_i, for $i=1\dots,N$, to give* (20) *as the point where the hybridisation (between the N resonators) was performed (see also e.g. [5]).*

2.3 Numerical computations of resonant modes

In order to improve computational efficiency, we will assume from here onward that the cell bundles are circular. This means that we can use the so-called multipole expansion method, an explanation of which is provided in *e.g.* [6, Appendix C]. The method relies on the idea that functions in $L^2(\partial D)$ are, on each *circular* ∂D_i, 2π-periodic so we may approximate by the leading order terms of a Fourier series representation. We found that as few as seven terms was sufficient to give satisfactory results.

Using such an approach we can find, for each fixed $\delta>0$, the N values of $\omega\in\mathbb{C}$ such that there exists a nontrivial solution to (21). For the case where $N=50$ the results are shown in Figure 2. We see that there is a range of frequencies where the (the real part of the) resonances occur most commonly. As N is increased, the resonances become increasingly dense in this region. In fact, with the current arrangement, this range of frequencies does not change as N increases. Instead, the region becomes increasingly densely filled.

It is also seen from Figure 2 that the imaginary parts of the resonances is smallest in the region where they are most dense. This means that these frequencies experience the least significant attenuation, suggesting that tones in this range will be most easily audible. The reason $\omega_1 = 0.0002284 - 0.0000526i$ has been omitted from Figure 2 is due to its $O(10^{-4})$ imaginary part. This is not only inconvenient for plotting but also means that this resonant mode will

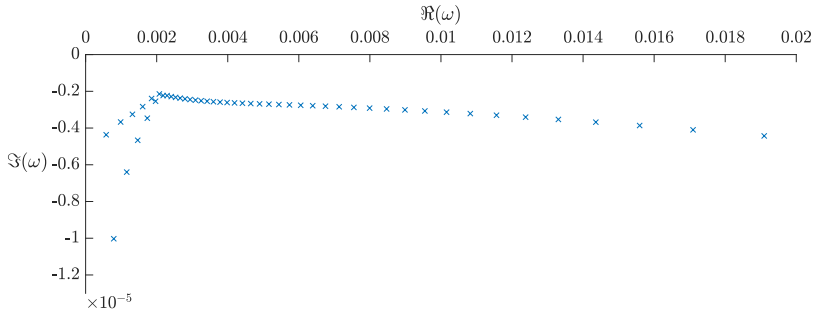

Figure 2: The resonant frequencies, plotted in the complex plane, of a system of 50 bundles arranged linearly with each being 1.05 times the size of the previous. The first resonance $\omega_1 = 0.0002284 - 0.0000526i$ is omitted. We take $\delta = 1/7000$ in this simulation.

suffer much greater attenuation and thus will be a less significant part of the motion over time.

It is also important to understand the eigenmodes u_n associated with each resonant frequency ω_n. The six resonant modes for the case of six cell bundles are shown in Figure 3. They take the form of increasingly oscillating patterns that inherit the asymmetry of the resonator array.

It is also notable that the solution is approximately constant on each bundle. This is because the solution, taking the form (9), is given by $\hat{\mathcal{S}}_D^{k_b}[\phi]$ at leading order which by Lemma 2.11 is constant for $\phi \in \ker(-\frac{1}{2}Id + \mathcal{K}_D^*)$.

The choice of size factor 1.05 in Figures 2 & 3 is made purely for convenience. In a real cochlea the number would be somewhat closer to 1 however, since we lack the computational power to model the full organ (with several thousand hair cells), a slightly larger value is used in order to make the observable behaviour clearer to the reader. The data from [22] suggests that in a real cochlea this value would be approximately[†] 1.0004.

2.4 Signal processing

We wish to offer an explanation of how, given an incident wave $p^{in}(x,t)$, our system of coupled resonators is able to classify (and hence identify) the sound. The system of resonators D is able to decompose the signal over its resonant modes. It is clear that the N eigenmodes are linearly independent so we may define the relevant N-dimensional solution spaces.

Definition 2.15. *We define the N-dimensional spaces X and Y as*

$$X := span\{u_1(x), \dots, u_N(x)\}, \tag{22}$$

$$Y := span\{u_1(x)e^{-i\omega_1 t}, \dots, u_N(x)e^{-i\omega_N t}\}, \tag{23}$$

[†]Based on the assumption that 3500 hair cells increase in size from 20µm to 70µm.

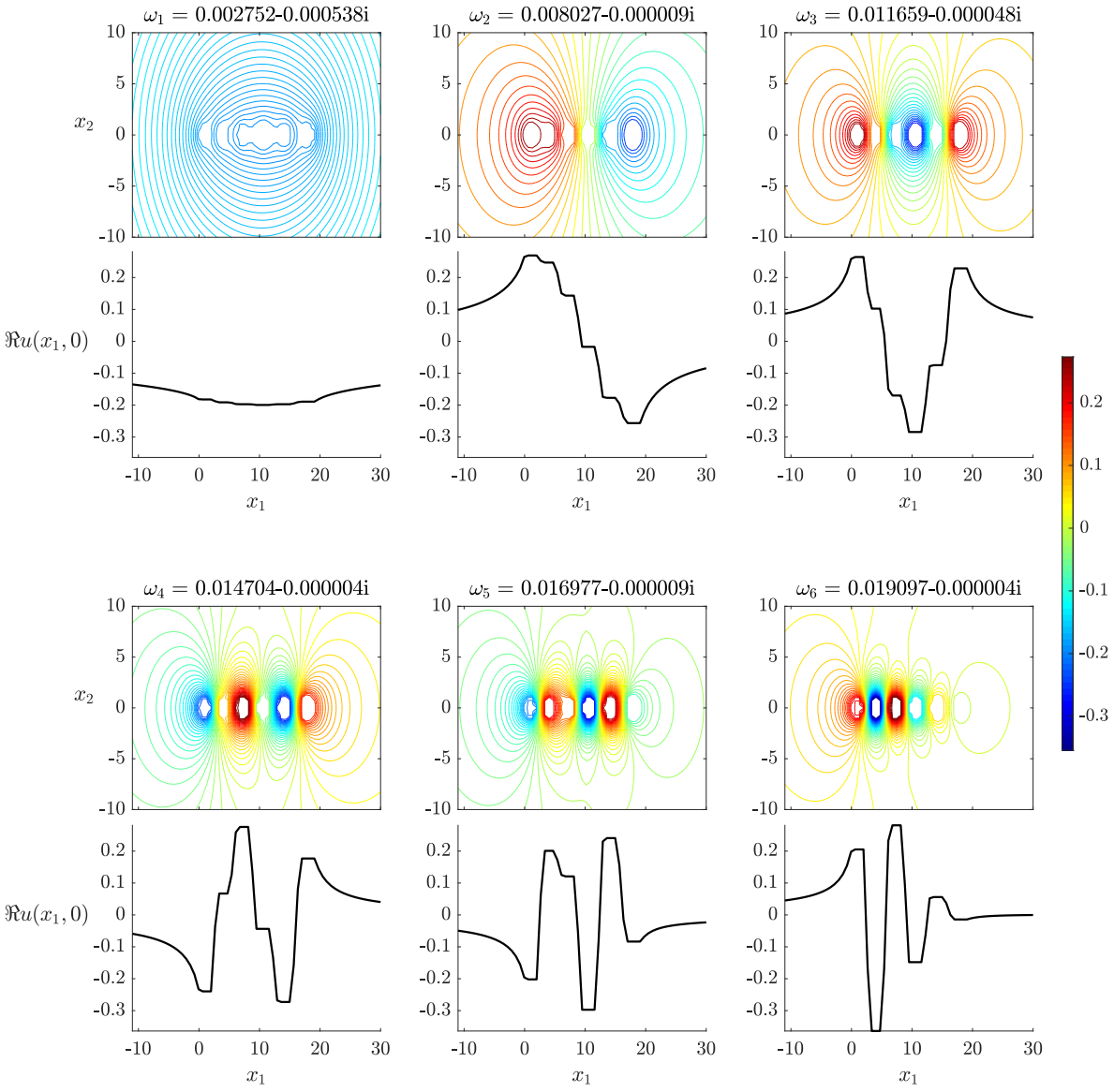

Figure 3: The acoustic pressure eigenmodes $u_1, \ldots, u_6$ for a system of six cell bundles arranged linearly with each being 1.05 times the size of the previous (smallest on the left). Each pair of plots corresponds to one of the six resonant frequencies. The upper plot shows a contour plot of the function $\Re u_n(x_1, x_2)$. The lower plot shows the cross section of this, taken along the line $x_2 = 0$ (*i.e.* through the centres of the bundles). The eigenmodes have been normalised such that $\int_D |u_n|^2 \, dx = 1$ for each $n = 1, \ldots, N$.

We will approximate the solution by a decomposition in the frequency domain. The fact that, for $n = 1, \ldots, N$, the Fourier transform of $e^{-i\omega_n t}$ for $t > 0$ is given by $i/(\omega - \omega_n)$ motivates us to employ the form

$$u(x, \omega) \simeq \sum_{n=1}^{N} \frac{\alpha_n(\omega) i}{\omega - \omega_n} u_n(x), \tag{24}$$

where $\alpha_1, \ldots, \alpha_N$ are complex-valued functions of a real variable.

It is important to understand whether knowing the value of the solution on each cell bundle (which is the information that a cochlea is able to capture) means that one can recover the weight functions $\alpha_1, \ldots, \alpha_N$ in (24).

Remark 2.16. *The eigenmodes $u_1, \ldots, u_N$ are not orthogonal in $L^2(D)$.*[†]

Proposition 2.17. *Let $\{\omega_1, \ldots, \omega_N\}$ be the resonances of the system $D = D_1 \cup \ldots \cup D_N$ and denote by $u_1, \ldots, u_N$ the corresponding eigenmodes. Then the matrix $\gamma \in \mathbb{C}^{N \times N}$ defined by*

$$\gamma_{ij} := \int_D u_i(x) \overline{u_j(x)}\, dx \quad i, j = 1 \ldots N, \tag{25}$$

is invertible.

Proof. We can apply the Gram-Schmidt procedure to produce a basis $\{v_1, \ldots, v_N\}$ for X that is orthonormal with respect to $(\cdot, \cdot)_{L^2(D)}$. This procedure produces a nonsingular lower triangular matrix $P \in \mathbb{C}^{N \times N}$ such that $(v_1, \ldots, v_N)^T = P(u_1, \ldots, u_N)^T$ (superscript T denotes the matrix transpose). If we define $Q \in \mathbb{C}^{N \times N}$ as $Q := P^{-1}$ then Q is also nonsingular and lower triangular. We can then calculate that

$$\begin{bmatrix} u_1 & \ldots & u_N \end{bmatrix}^T \begin{bmatrix} \overline{u_1} & \ldots & \overline{u_N} \end{bmatrix} = Q \begin{bmatrix} v_1 & \ldots & v_N \end{bmatrix}^T \begin{bmatrix} \overline{v_1} & \ldots & \overline{v_N} \end{bmatrix} \overline{Q}^T. \tag{26}$$

Integrating (26) componentwise gives that, for $i, j = 1, \ldots, N$, it holds that

$$\gamma_{ij} = \left[Q I_N \overline{Q}^T \right]_{ij}, \tag{27}$$

and thus

$$\det(\gamma) = |\det(Q)|^2 > 0. \tag{28}$$

□

In order to find the weight functions $\alpha_1, \ldots, \alpha_N$ in Equation (24) we must take the $L^2(D)$-product with $u_n(x)$ for $n = 1, \ldots, N$ and then invert γ. This gives that

$$\begin{pmatrix} \frac{\alpha_1(\omega) i}{\omega - \omega_1} \\ \vdots \\ \frac{\alpha_N(\omega) i}{\omega - \omega_N} \end{pmatrix} = \overline{\gamma}^{-1} \begin{pmatrix} (u(\cdot, \omega), u_1)_{L^2(D)} \\ \vdots \\ (u(\cdot, \omega), u_N)_{L^2(D)} \end{pmatrix}. \tag{29}$$

[†]It turns out however that they are *nearly* orthogonal. For example, the normalised eigenmodes shown in Figure 3 satisfy $(u_n, u_m)_{L^2(D)} = O(10^{-3})$ for $n \neq m$.

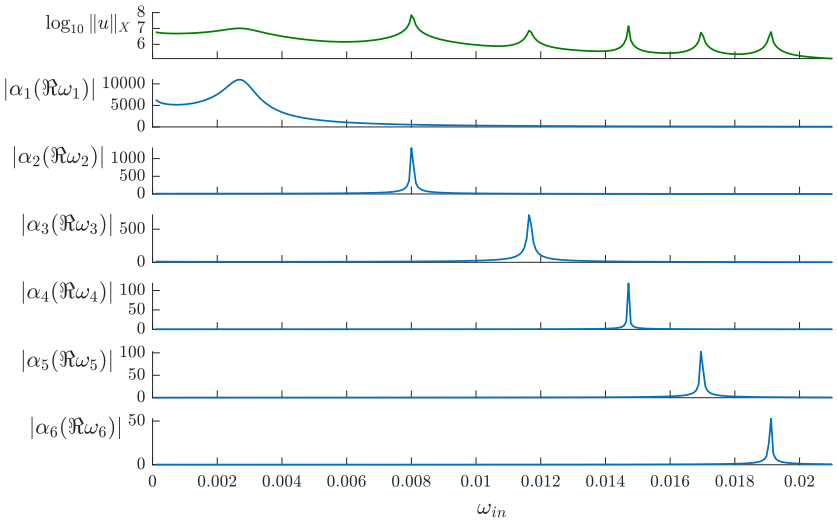

Figure 4: A system of six cell bundles filters an acoustic signal into the six resonant frequencies. We consider a system of six linearly arranged circular cell bundles that increase in size by a factor of 1.05 which is subjected to an incoming plane wave with frequency ω_{in}. The first plot shows how the norm of the solution $u(x,\omega)$ to (5) varies as a function of ω_{in}. We then show how each coefficient $\alpha_1(\omega_1),\ldots,\alpha_N(\omega_N)$ in (30) varies. The six resonant frequencies of this system are $\omega_1 = 0.002752 - 0.000538i$, $\omega_2 = 0.008026 - 0.000009i$, $\omega_3 = 0.011659 - 0.000048i$, $\omega_4 = 0.014703 - 0.000004i$, $\omega_5 = 0.016976 - 0.000009i$, $\omega_6 = 0.019096 - 0.000004i$.

Thanks to its representation (9) in terms of single layer potentials, $u(\cdot,\omega)$ is an analytic function of $\omega \in \mathbb{C}$. Thus, from (29) we can see that $\alpha_1,\ldots,\alpha_N$ are analytic and hence we can recover a similar decomposition for $p(x,t)$ using the Laplace inversion theorem

$$\begin{aligned} p(x,t) &\simeq \frac{1}{2\pi}\sum_{n=1}^{N} u_n(x)\int_{-\infty}^{\infty}\frac{\alpha_n(\omega)i}{\omega-\omega_n}e^{-i\omega t}\,d\omega \\ &= \sum_{n=1}^{N} u_n(x)\alpha_n(\omega_n)e^{-i\omega_n t}, \quad t>0. \end{aligned} \tag{30}$$

Example 2.18. *$p^{in}(x,t)$ is a plane wave*

We take as an example the case where $p^{in}(x,t)$ is a pulse of a plane wave with frequency $\omega_{in} \in \mathbb{R}$ travelling in the x_1 direction. This is given by

$$p^{in}(x,t) = e^{i\omega_{in}(x_1/v-t)}, \quad 0<t<1. \tag{31}$$

This has Fourier transform

$$u^{in}(x,\omega) = 2e^{\frac{i}{2}(\omega-\omega_{in})}\mathrm{sinc}(\omega-\omega_{in})e^{i\omega_{in}x_1/v}. \tag{32}$$

We can then compute $\alpha_1(\omega),\ldots,\alpha_N(\omega)$ as in (29).

In Figure 4 we show firstly how the $L^2(D)$-norm of the solution to the scattering problem (5) varies as a function of ω_{in}. As is expected, the response is (locally) much greater when ω_{in} is close to $\Re(\omega_n)$ for some $n = 1, \ldots, N$. We also show how the weights $\alpha_1(\omega_1), \ldots, \alpha_N(\omega_N)$ in (30) vary as a function of ω_{in}. Each constant is small except in a region of the associated resonant frequency when the corresponding eigenmode is excited most strongly.

It should also be noted that $|\alpha_n(\omega_n)|$ decreases in n. If we considered higher order resonances the corresponding constants would be significantly smaller. This justifies our choice to approximate p as an element of Y in (30) (*i.e.* to only consider the N subwavelength modes).

2.5 Travelling waves

In trying to resolve the differences between the two main classes of cochlear model a crucial realisation is that our (resonance) model for the acoustic pressure exhibits the travelling wave behaviour. This is easy to see in models based on graded arrays of *uncoupled* resonators, since a resonator's response time increases with decreasing characteristic frequency [11, 16], but is also true of our hybridised model.

While it is true that acoustic waves enter the cochlea at the base and travel through the fluid to the apex, the wave observed by Békésy moves much more slowly than this. The speed of sound in cochlea fluid is approximately $1500\mathrm{m\,s^{-1}}$ whereas the travelling wave is observed at speeds close to $10\mathrm{m\,s^{-1}}$[11, 14]. This justifies the assumption that all the hair cells are excited simultaneously by an incoming signal (see *e.g.* [11]). Under this assumption, exciting an array initially at rest produces the evolution shown in Figure 5, from which the existence of a wave travelling from the small high-frequency resonators at the base of the cochlea to the larger

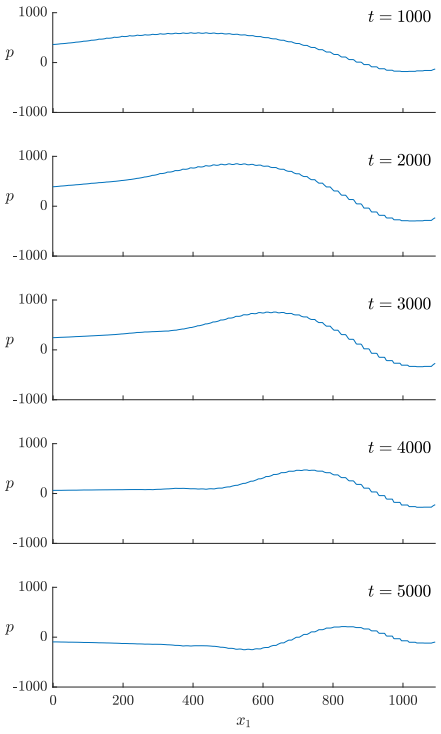

Figure 5: Our graded resonance model exhibits travelling wave behaviour in the pressure field. We show the evolution over time of the acoustic pressure $p = p((x_1, 0), t)$ scattered by 50 evenly spaced circular cells (with size increasing by a factor of 1.05 from left to right). The acoustic pressure is initially zero then the cells are simultaneously excited at $t = 0$. We plot the cross-section of the field along $x_2 = 0$ (through the centres of the cell bundles).

low frequency resonators at the apex is clear. This wave is merely the movement of the position of maximum acoustic pressure along the array of resonators. It is a consequence of the asymmetric eigenmodes growing from rest at different rates.

It is clear from Figure 5 that the amplitude initially increases before quickly decreasing as the wave moves through the cochlea. This is notably consistent with Békésy's waves on the membrane [16, 24] and is to be expected in light of the $e^{-i\omega_n t}$ factors ($\Im(\omega_n) < 0$) in (30). It is observed (in humans) that the travelling wave slows down as it moves through the cochlea [14] which is also witnessed in Figure 5: the position of the wave moves relatively little between the third and fifth plots.

2.6 Tonotopic map

Von Békésy's famous experiments further revealed the existence of a relationship between signal frequency and the position in the cochlea where the sound is most strongly detected. His results showed that the frequency $f(x)$ giving rise to maximum excitation at a distance x from the base of the cochlea satisfies a tonotopic map of the form

$$f(x) = ae^{-x/d} + c, \tag{33}$$

for some $a, d, c \in \mathbb{R}$ [24]. In Figure 6 we show the relationship between the position of maximum amplitude of each eigenmode and the associated resonant frequency. We see that, if some of the lowest frequency modes are ignored, the pattern follows a relationship that is approximately of the form (33) (with $a = 0.0126, d = -0.0117, c = 0.0060$). The eigenmodes shown in Figures 6b-d demonstrate the basis for the tonotopic map. Each features oscillations with a clear peak followed by a rapid decrease in amplitude.

It is not clear why the lowest frequency modes (*e.g.* Figure 6a) do not fit the pattern that is established by the majority of the eigenmodes, or what the implications of this are. However the relatively large negative imaginary parts of the associated resonant frequencies mean this phenomenon has a less significant impact on the evolution of the acoustic pressure field.

The shape of the eigenmodes in Figures 6b-d further provides a basis for the growth and then rapid decay of the travelling wave that was observed in Figure 5.

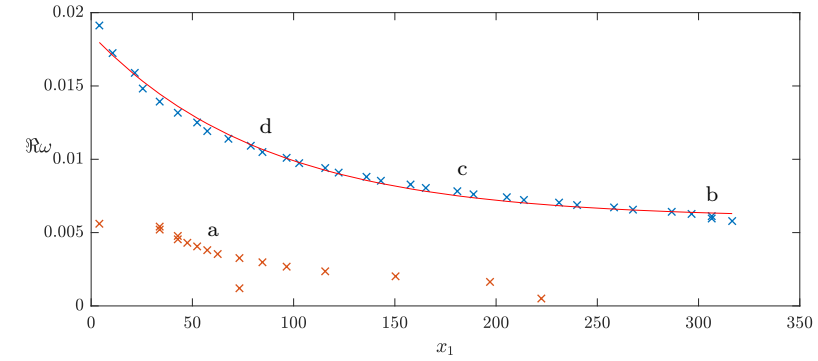

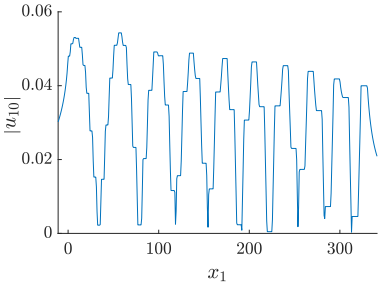

(a) $\omega_{10} = 0.003803 - 0.000003i$

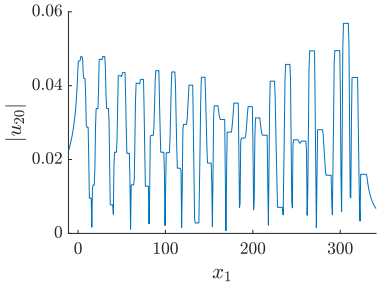

(b) $\omega_{20} = 0.006122 - 0.000001i$

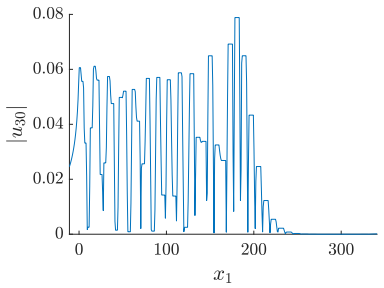

(c) $\omega_{30} = 0.007612 - 0.000001i$

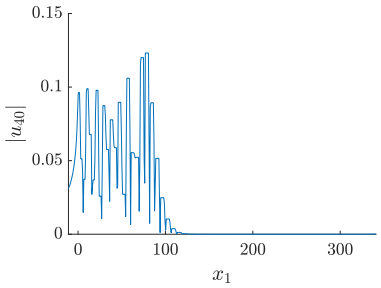

(d) $\omega_{40} = 0.01049 - 0.000002i$

Figure 6: The existence of a tonotopic map for a passive system of graded oscillators. The top plot shows, for each eigenmode, the relationship between the real part of the associated resonant frequency $\Re\omega$ and the location (x_1-coordinate) of the maximum amplitude. We study the case of 50 cells, increasing in size by a factor of 1.05 from left to right. A (least squares) approximation to the relationship exhibited by the blue points is shown, this has equation $0.0126e^{-0.0117x} + 0.0060$. The 17 orange points are excluded from this calculation.
(a)-(d) are the eigenmodes corresponding to the points marked on the top plot. We depict the absolute value of each eigenmode $|u_n| = |u_n(x_1, 0)|$ along the line $x_2 = 0$ (through the centres of the cells). It should be noted that the eigenmodes quickly decrease to zero outside of the region where the cells are located.

3 Concluding remarks

In this paper, we have computed leading order approximations to the resonant frequencies and associated eigenmodes for a system of coupled subwavelength acoustic oscillators that are graded in size. This model has the ability to decompose incoming signals into these resonant modes. It is a significant observation that the graded resonance model predicts the travelling wave behaviour in the acoustic pressure field, contributing to the unification of Helmholtz' and Békésy's models [11].

On the other hand, it is well known that the cochlea is an active organ [13, 18–20, 23]. For instance, a key feature that our current model lacks is the ability to amplify quiet sounds more greatly than louder ones. Such nonlinear amplification is needed in order to account for the ear's remarkable ability to hear sounds over a large range of amplitudes. In future work we will investigate how introducing appropriate nonlinear forcing terms in (1) can produce the desired amplification as well as further enhance the model's frequency selectivity.

Acknowledgement.

The authors are grateful to Fabrice Lemoult for their participation in valuable discussions.

References

[1] Allen, J. (2001). Nonlinear cochlear signal processing. In *Physiology of the Ear, Second Edition*, pages 393–442. Singular Thompson, San Diego.

[2] Ammari, H., Ciraolo, G., Kang, H., Lee, H., and Yun, K. (2013). Spectral analysis of the neumann–poincaré operator and characterization of the stress concentration in anti-plane elasticity. *Arch. Ration. Mech. An.*, 208(1):275–304.

[3] Ammari, H., Fitzpatrick, B., Gontier, D., Lee, H., and Zhang, H. (2018a). Minnaert resonances for acoustic waves in bubbly media. *Ann. I. H. Poincaré–An.*, 35(7):1975–1998.

[4] Ammari, H., Fitzpatrick, B., Kang, H., Ruiz, M., Yu, S., and Zhang, H. (2018b). *Mathematical and computational methods in photonics and phononics*, volume 235 of *Mathematical Surveys and Monographs*. American Mathematical Society, Providence.

[5] Ammari, H., Fitzpatrick, B., Lee, H., Yu, S., and Zhang, H. (2017a). Double-negative acoustic metamaterials. *arXiv preprint arXiv:1709.08177*.

[6] Ammari, H., Fitzpatrick, B., Lee, H., Yu, S., and Zhang, H. (2017b). Subwavelength phononic bandgap opening in bubbly media. *J. Differ. Equations*, 263(9):5610–5629.

[7] Ammari, H. and Kang, H. (2004). Boundary layer techniques for solving the Helmholtz equation in the presence of small inhomogeneities. *J. Math. Anal. Appl.*, 296(1):190–208.

[8] Ammari, H. and Kang, H. (2007). *Polarization and moment tensors: with applications to inverse problems and effective medium theory*, volume 162. Springer Science & Business Media.

[9] Ammari, H., Kang, H., and Lee, H. (2009). *Layer potential techniques in spectral analysis*, volume 153 of *Mathematical Surveys and Monographs*. American Mathematical Society, Providence.

[10] Ammari, H. and Zhang, H. (2015). A mathematical theory of super-resolution by using a system of sub-wavelength Helmholtz resonators. *Commun. Math. Phys.*, 337(1):379–428.

[11] Bell, A. (2012). A resonance approach to cochlear mechanics. *PLoS One*, 7(11):e47918.

[12] Bell, J. A. (2005). *The underwater piano: a resonance theory of cochlear mechanics*. PhD thesis, The Australian National University.

[13] Crawford, A. and Fettiplace, R. (1985). The mechanical properties of ciliary bundles of turtle cochlear hair cells. *J. Physiol.*, 364(1):359–379.

[14] Donaldson, G. S. and Ruth, R. A. (1993). Derived band auditory brain-stem response estimates of traveling wave velocity in humans. i: Normal-hearing subjects. *J. Acoust. Soc. Am.*, 93(2):940–951.

[15] Duifhuis, H. (2012). *Cochlear mechanics: introduction to a time domain analysis of the nonlinear cochlea*. Springer Science & Business Media, New York.

[16] Fletcher, N. H. (1992). *Acoustic systems in biology*. Oxford University Press, New York.

[17] Hudspeth, A. J. (1983). The hair cells of the inner ear. *Sci. Am.*, 248(1):54–65.

[18] Kemp, D. T. (1978). Stimulated acoustic emissions from within the human auditory system. *J. Acoust. Soc. Am.*, 64(5):1386–1391.

[19] Kemp, D. T. (2008). Otoacoustic emissions: concepts and origins. In *Active processes and otoacoustic emissions in hearing*, pages 1–38. Springer, New York.

[20] Moller, A. R. (2000). *Hearing: its physiology and pathophysiology*. Academic Press, San Diego.

[21] Olson, E. S. (1999). Direct measurement of intra-cochlear pressure waves. *Nature*, 402(6761):526.

[22] Pujol, R., Lenoir, M., Ladrech, S., Tribillac, F., and Rebillard, G. (1992). Correlation between the length of outer hair cells and the frequency coding of the cochlea. In *Auditory physiology and perception*, pages 45–52. Pergammon, Oxford.

[23] Shera, C. A. (2003). Mammalian spontaneous otoacoustic emissions are amplitude-stabilized cochlear standing waves. *J. Acoust. Soc. Am.*, 114(1):244–262.

[24] Von Békésy, G. and Wever, E. G. (1960). *Experiments in hearing*, volume 8. McGraw-Hill, New York.

[25] Von Helmholtz, H. L. F. (1875). *On the sensations of tone as a physiological basis for the theory of music*. Longmans, Green, London.